Available online at www.sciencedirect.com
SCIENCE DIRECT®
Journal of Solid State Chemistry 176 (2003) 575–586
JOURNAL OF SOLID STATE CHEMISTRY
http://elsevier.com/locate/jssc

Quantum chemical contributions on the reactivity of solids

Karl Jug* and Gerald Geudtner

Theoretische Chemie, Universität Hannover, Am Kleinen Felde 30, 30167 Hannover, Germany

Received 9 January 2003; received in revised form 30 May 2003; accepted 4 June 2003

Abstract

The concept of reactivity is reviewed. Various reactivity indices are discussed. Different methods for the simulation of solids are systematically described. Applications for the reactivity of solids can be subdivided into three categories: surfaces, interfaces and bulk. Examples for the categories are presented with a special emphasis on diffusion processes in the bulk.

1. Concept of reactivity

Chemical reactivity is one of the essential concepts of chemistry. The more it is surprising that this notion remains somewhat elusive. If we consult an encyclopedia of chemistry [1] and search for the term "reactivity" we get a cross reference to "reaction", where we find at the end of this term the following explanation: In particular quantum chemistry contributes to the understanding of the reactivity of chemical elements by predictions of the possible reaction behaviour of molecules via perturbation, theoretical and other computational procedures of molecular orbital theory.

Of course, the notion of "reactivity" and "reaction" are intimately related. Whereas reactivity is the capability to react, i.e., a property of the reacting system or systems, and provides an implicit prediction of a reaction, the reaction itself is the explicit process via a reaction pathway (Fig. 1). The initiation of the reaction by the reactants is usually described by reactivity indices, whereas the reaction as a whole is described by its energetics.

There are different kinds of reactivity: (i) reactivity of atoms, e.g., in substitution reactions, (ii) reactivity of bonds, e.g., in addition reactions, (iii) reactivity of vacancies, e.g., in diffusion processes. Whereas the first two are generally valid for molecules and solids alike, the third is typical only for solids.

The description of reactivity is related to bond forming, bond breaking and can involve migration of atoms or charge transfer.

To quantify reactivity, reactivity indices have been defined. These are related, e.g., to atomic net charge, atomic dipole moments, atomic valence, bond valence, chemical potential, hardness or electrostatic potential. However, the most direct measure is activation energy (kinetic effect) and product stability (thermodynamic effect). The relation to solids is via surfaces and interfaces, in particular defects like steps, edges and corners. Vacancies and lattice defects are responsible for the reactivity in the bulk.

2. Reactivity of molecules

The quantification of reactivity via reactivity indices has a long history. Svartholm [2] calculated electronic charge distributions in condensed unsaturated hydrocarbons in the framework of valence bond (VB) theory. He recognized two different competing kinds of reactivity: reactivity at atoms and reactivity at bonds. Reactivity was connected with the distribution of the π electrons, in particular with their shift between the atoms. Daudel and Pullman [3] improved this approach and achieved a comparison of reactivity between sites in different molecules. A few years later the expression "free valence" was introduced [4]. The other major approach to reactivity was on the level of molecular orbital (MO) theory. Coulson [5] derived charge and bond orders in the framework of an energy expression at

*Corresponding author. Fax: +49-511-7625939.
E-mail address: jug@mbox.theochem.uni-hannover.de (K. Jug).

0022-4596/$ - see front matter © 2003 Elsevier Inc. All rights reserved.
doi:10.1016/S0022-4596(03)00338-4

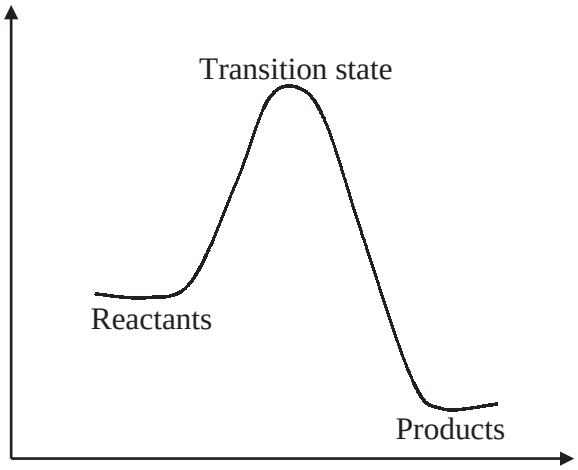

Fig. 1. Typical reaction pathway for a chemical reaction.

the level of the Hückel method. The π electrons were considered explicitly and the σ electrons were considered as a non-polarizable core. The valence number N_A of an atom A was defined as the sum of all bond orders of neighbor atoms B, which were bound to reference atom A. It was postulated that a maximum valence number could be obtained depending on the nature of the atom and the state of hybridization. Free valence F_A of an atom was then introduced as the difference between the maximum valence and the actual valence of an atom in a molecule

$$F_A = N_{A\,\max} - N_A. \tag{1}$$

Coulson's approach worked best for a free-radical attack [6,7], but could fail for electrophilic or nucleophilic attack because the direct influence of atomic net charge was completely disregarded.

It was up to Fukui [8] to recognize the importance of the frontier orbitals. The electronic distribution of the highest occupied molecular orbital (HOMO) is most essential for an electrophilic attack. Correspondingly, the lowest unoccupied molecular orbital (LUMO) is important for nucleophilic attack [9]. In a radical reaction the highest singly occupied molecular orbital (SOMO) must be considered. The three different situations are depicted in Fig. 2. The feasibility of the nucleophilic reaction depends on the efficiency of the transfer of electrons from the HOMO of the reagent to the unoccupied molecular orbital LUMOs of the reactant. Likewise, the transfer of electrons from the occupied molecular orbitals (OMOs) of the reactant to the LUMO of the reagent is essential. In the case of the radical attack, both charge transfer from the OMOs of the reactant to the SOMO of the reagent and/or from the SOMO of the reagent to the UMOs of the reactant must occur. The explicit form of Fukui's reactivity index for the three types of reactions is too simple to distinguish explicitly between covalent and ionic influences on the reactivity. Such an approach must take care of the fact that charge transfer is limited. An atom will favor acquisition of charge in nucleophilic attack only up to a point where it reaches its normal charge, i.e., the charge of the free atom. If its net charge is already negative, it will resist charge transfer and the value of the reactivity index must be reduced. Such a scheme has been devised [10] where valence and charge differences are considered so that the reactivity index R can be formulated as

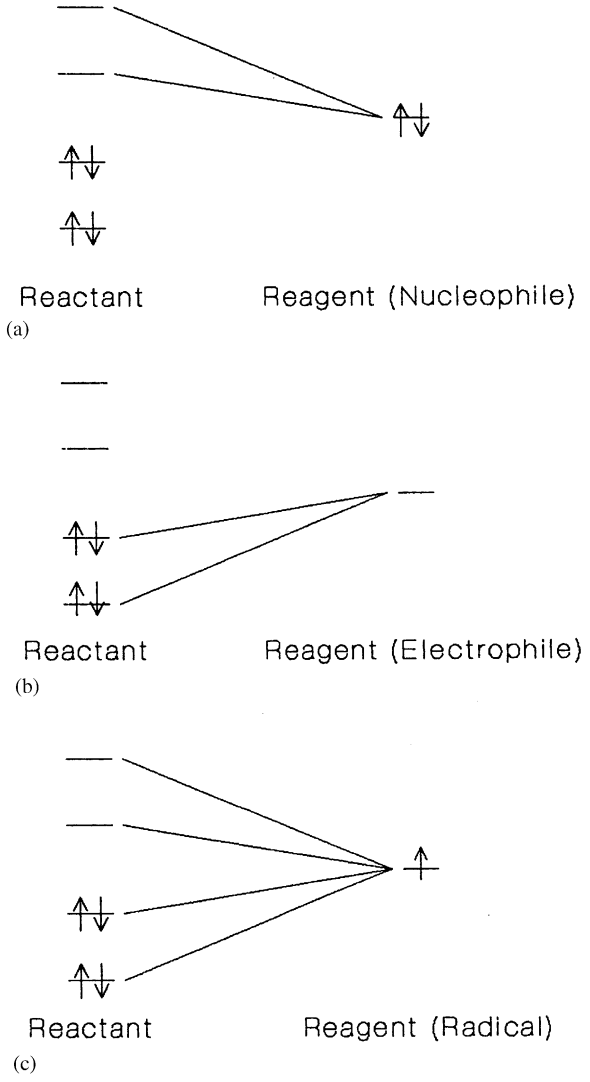

Fig. 2. Important orbitals for reactions with (a) nucleophilic, (b) electrophilic and (c) radical reagents.

$$R = R_{\text{covalent}} + R_{\text{ionic}}. \tag{2}$$

R_{covalent} measures the valence differences [11] of atoms in the ground state and dianion (dication) state of the reactant in a nucleophilic (electrophilic) reaction. R_{ionic} measures the charge differences of the corresponding states. A radical attack requires a modified combination of nucleophilic and electrophilic attack.

All these approaches serve to interpret the initiation of the chemical reaction. They are concerned with the pretransition stage, but only to some extent indirectly with the post-transition stage. They do not describe explicitly the relative stability of the product.

Density functional theory (DFT) gave a new impact to the theory of reactivity. Parr and Pearson [12] derived the concept of absolute hardness via derivatives of the energy E with respect to the number of electrons N of a system. The first derivative is defined as the chemical potential μ

$$\mu = (\partial E/\partial N)_Z = -\chi, \tag{3}$$

where Z is the total number of nuclear charges in a molecule. μ is the negative of the electronegativity χ of the system. The hardness η is defined as the second derivative

$$\eta = \frac{1}{2}(\partial^2 E/\partial N^2)_Z. \tag{4}$$

Hardness is meant to be the resistance of the chemical potential to change in the number of electrons. The inverse of hardness is softness [13]:

$$S = \frac{1}{2\eta}. \tag{5}$$

In the finite difference approximation, one can write

$$\mu \approx -\frac{1}{2}(I + A),$$
$$\eta \approx \frac{1}{2}(I - A). \tag{6}$$

As usual I is the ionization potential and A the electron affinity. These quantities served to apply the hard–soft acid–base (HSAB) principle by Pearson [14]. Shortly after the definition of hardness, Parr and Yang [15] rationalized the frontier orbital theory of Fukui from density functional theory. They introduced a reactivity index $f(\mathbf{r})$ as the variation of the chemical potential μ with respect to the external potential $v(\mathbf{r})$:

$$f(\mathbf{r}) = (\delta\mu/\delta v(\mathbf{r}))_N. \tag{7}$$

$f(\mathbf{r})$ was called the Fukui function. Alternatively, $f(\mathbf{r})$ can be rewritten as the partial derivative of the density $\rho(\mathbf{r})$ with respect to the number N of electrons via a Maxwell relation

$$f(\mathbf{r}) = (\partial\rho(\mathbf{r})/\partial N)_v. \tag{8}$$

The three cases of reactivity toward a nucleophilic attack, an electrophilic attack and a radical attack of a reagent can be described by the three Fukui functions $f^+(\mathbf{r})$, $f^-(\mathbf{r})$ and $f^0(\mathbf{r})$, respectively, which are approximated by

$$f^+(\mathbf{r}) \approx \rho_{\mathrm{LUMO}}(\mathbf{r}),$$
$$f^-(\mathbf{r}) \approx \rho_{\mathrm{HOMO}}(\mathbf{r}),$$
$$f^0(\mathbf{r}) \approx \frac{1}{2}[\rho_{\mathrm{HOMO}}(\mathbf{r}) + \rho_{\mathrm{LUMO}}(\mathbf{r})]. \tag{9}$$

As related quantities the local softness $s(\mathbf{r})$ and the local hardness $\eta(\mathbf{r})$ were introduced [16].

Another approach to chemical reactivity is via the application of molecular electrostatic potentials (MESP) [17,18]. The molecular electrostatic potential is defined as

$$V(\mathbf{r}) = V_{\mathrm{n}}(\mathbf{r}) + V_{\mathrm{e}}(\mathbf{r}) = \sum_A \frac{Z_A}{|R_A - \mathbf{r}|} + \int \frac{\rho(\mathbf{r}')}{|\mathbf{r} - \mathbf{r}'|}\,\mathrm{d}\mathbf{r}'. \tag{10}$$

It consists of a nuclear part (n) and an electronic part (e) and describes the effect of nuclear and electronic charges at a point $\mathbf{r}$. By definition it is a real physical quantity which is measurable. By computing contour maps of the MESP in selected planes through a molecule regions of negative and positive MESP can be identified. Its relation to chemical reactivity stems from the fact that regions of negative MESP would be favored for electrophilic attack and regions of positive MESP would be favored in a nucleophilic attack. This is particularly true in the initiation phase of a reaction where a reagent is approaching a reactant. The emphasis is here on the electrostatic interaction. Such a reactivity description is therefore purely static, because the response of the system is not included. For a dynamic description the structural and electronic relaxation during a reaction have to be considered.

All the presented reactivity indices can not only be applied to molecules, but equally well to solids.

3. Simulation of solids

Solids can be simulated in different ways. Fig. 3 contains an overview on various simulation approaches. From the molecular starting point it is clear that the free cluster approach is the most natural. Considering two kinds of atoms A and B, the arrangement of the atoms would be chosen as a cut out of the crystal lattice in the solid state. The cluster approach is particularly useful, if the structure of the optimized finite clusters is similar to that of the bulk. Of course, the borders of the clusters would be somewhat deformed in a structure optimization process. In order to reduce such a border effect, the size of the cluster has to increased sometimes significantly beyond that of normal molecules and the bulk structure has to be maintained. We have used this approach frequently in the past starting with NaCl and MgO clusters [19]. To avoid the increase of clusters for the description of solids, saturated clusters have been quite popular. Here atoms of low coordination number, in particular hydrogen atoms have been used to saturate the borders of the free cluster. There is also a need for saturation, if the structure of the clusters and the structure of the bulk differs significantly as is the case

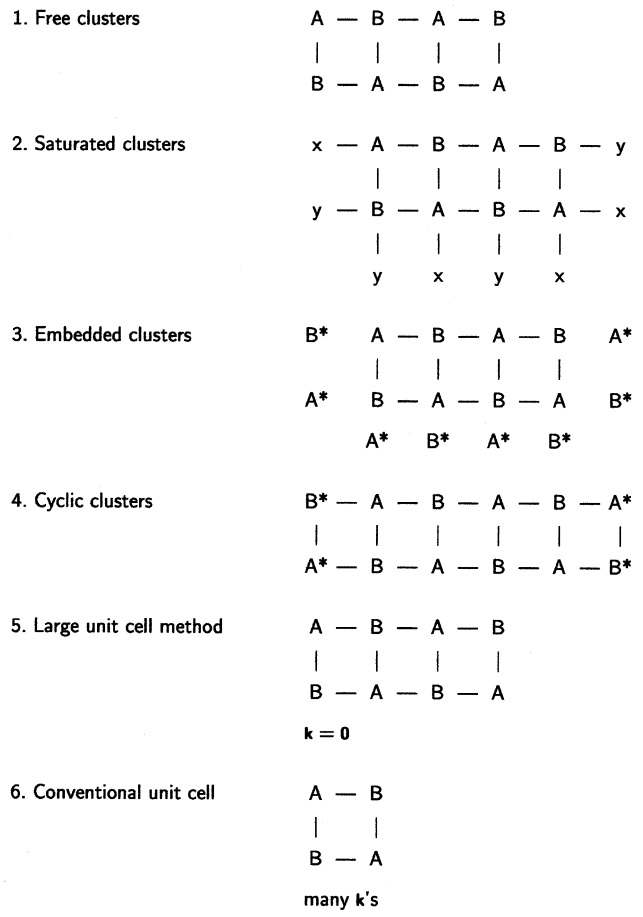

Fig. 3. Various approaches to the simulation of solids.

for silicon clusters [20]. The choice of a completly different kind of atoms for saturation compared to the real cluster atoms is of course unsatisfactory. It is therefore only consequential to introduce an embedding procedure. For ionic compounds point charges are widely in use. However, the introduction of pseudo atoms A^* and B^* which are the same kind and act on a system of real atoms A and B via energy terms in the Fock matrix of the free cluster offers a much improved description [21]. However, the border problem is not ideally solved. There are still charge fluctuations in the real cluster, which would not be present in the bulk. To avoid these a periodic model must be introduced. The cyclic cluster model is such an approach. It has been recently revived [22] and extended to ionic systems [23]. In this approach a finite periodicity of a cluster is achieved by translations of real cluster atoms A and B from left to right and from right to left so that they constitute as atom A^* and B^* the same environment for the border atoms or the adjacent inner real atoms as for the real atoms in the center of the cluster. To avoid the limitations of a finite system, the cyclic cluster can in turn be embedded in an infinite Madelung potential [24]. A periodic approach is also the large unit cell method [25,26]. It represents an approach where the wave vector $\mathbf{k}$ is limited to $\mathbf{0}$. To compensate this restriction the conventional unit cell is enlarged. This procedure avoids a complex coefficient matrix, which is inherent in the conventional unit-cell approach. In the latter the reciprocal space of wave vectors is explicitly considered [27].

The various kinds of approaches to solids from finite non-periodic methods to finite periodic methods without and with embedding and finally to infinite periodic methods offer a variety of descriptions which have advantages for special situations. Whereas periodic methods are advantegeous for the treatment of ideal crystals, non-periodic methods are preferable for systems with defects.

4. Reactivity of solids

Reactivity of solids can be observed at surfaces and interfaces and in the bulk. Surface reactivity is usually related to a multi-component system where the solid surface is open for reaction with a gas or/and a liquid. The surface roughness expressed via corners, edges and steps plays an important role. A high mobility of one component is also required. Interfaces can occur in solids consisting of one- or two-component systems. Grain size, surface roughness and crystal planes have to be considered for reactivity. Reactivity of the bulk is related to crystal defects. It can be described indirectly by reactivity indices or by models of reaction steps or directly by a study of the reaction process. High mobility of defects implies fast diffusion. This can be explicitly described by molecular dynamics simulation which involves temperature and time in addition to energy. Finally pressure can be simulated by change of the cell volume.

4.1. Surfaces

4.1.1. Indices

To understand the reactivity of solids it seems natural to start with the reactivity of surfaces, because solid-state reactions often start at surfaces. The difference between the reactivity of molecules and the reactivity of surfaces can be easily explained in the case of silicon clusters versus silicon surfaces. Solid silicon shows dissociative adsorption of ammonia at room temperature both for the (2×1) reconstructed Si (100) surface and the (7×7) Si (111) surface [28–30]. In contrast, silicon clusters up to 70 atoms chemisorb ammonia without dissociation [31]. Their reactivity is smaller by an order of magnitude than that of solid silicon [32]. The large reactivity difference is surprising since small and medium clusters consist only of surface atoms which are not saturated and therefore possess numerous dangling

bonds at the surface. A probing of the reactivity of Si_5 and Si_{10} clusters revealed that reactive sites are the corners (atoms), not the edges (bonds) or surfaces of the cluster (Fig. 4) [33]. The preference of the different atomic sites could not be explained by net charges, rather the atomic dipole moments had to be considered, which originates from an anisotropy of the charge distribution at the cluster atoms. Alternatively, the MESP around the silicon clusters can be calculated [34]. Sites with positive MESP values are preferable for nucleophilic attack, whereas sites with negative MESP should prefer electrophilic reagents. The results for the reactivity of the Si_5 and Si_{10} clusters towards nucleophilic attack of NH_3 are qualitatively the same as for the dipole moment analysis, but the differences in the MESP values are very small. In the case of the Si (111) surface the unreconstructed surface (Fig. 5) shows sites with positive (black) and negative (gray) MESP. In contrast,

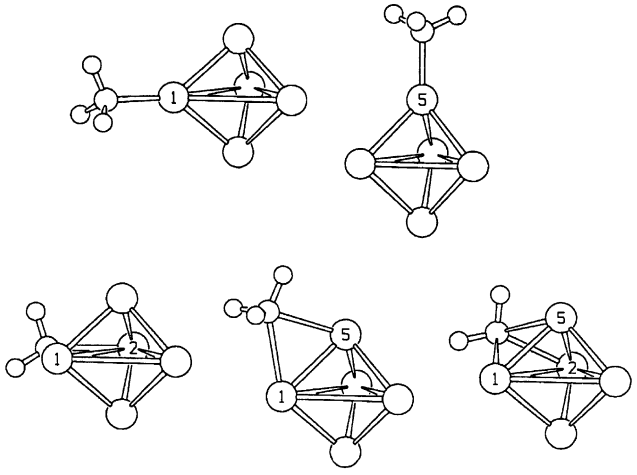

Fig. 4. Potential adsorption sites for ammonia on the Si_5 cluster surface

the reconstructed Si (111)-(7×7) surface shows a pronounced negative MESP [34] indicated by the white and light gray surface. This means that the reconstructed silicon surface has no electrophilic reactivity towards a nucleophilic attack of NH_3. Hence it favors adsorption of an H atom with subsequent bond breaking.

Another interesting system for surface chemistry is rutile (TiO_2). Its catalytic activity has frequently been explored, in particular for the dissociation of water. Here the charge sensitivity analysis by Nalewajski [35,36] is quite useful. This analysis extracts the reactivity indices from the semiempirical atom-in-molecules (AIM) hardness tensor

$$\eta_{ij} = \partial^2 E/\partial N_i \partial N_j = \partial \mu_i/\partial N_j = \partial \mu_j/\partial N_i \approx \gamma_{ij}, \tag{11}$$

where E is the electronic energy of the system, N_i denotes the local atomic electron population and γ_{ij} is the valence-shell Coulomb repulsion integral. The approximate equality was derived from an interpolation between asymptotic values for small and large internuclear distances. η_{ij} is approximated by the electronic repulsion and relates to the polarizability of the bond between atoms i and j. The preferred site for a nucleophilic attack is determined by the minimum of the AIM Fukui function

$$f_i = \partial N_i/\partial N, \tag{12}$$

where $N = \sum_i N_i$ is the global number of electrons. The preferred sites exhibit a negative Fukui function. Alternatively, an electrophilic reagent prefers a site with a positive Fukui function and the site with the maximum of f_i is the best. In Fig. 6 negative values of the Fukui function are given in black and positive values in white circles. The radius of the circle indicates the magnitude of the value. If we compare the Fukui functions for the TiO_2 (110) and (100) surfaces it is apparent that only the four-fold coordinated Ti atom, represented by the

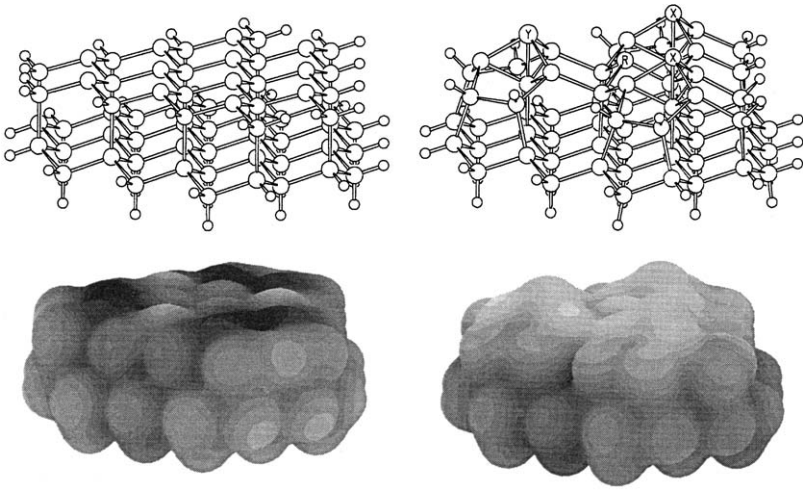

Fig. 5. Structure and MESP of the unreconstructed and reconstructed Si (1 1 1) surface.

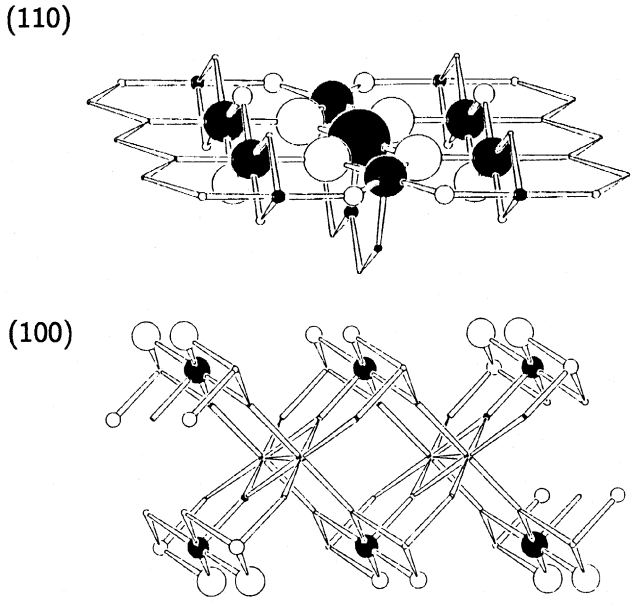

Fig. 6. Fukui functions of TiO_2 rutile (111) and (100) surfaces (black: negative, white: positive).

largest black circle of the (110) surface, offers a preferable site for a nucleophilic attack of a water molecule [37]. Due to the finite surface of the cluster the Ti atoms adjacent to the center atom have slightly different Fukui function values, which would be the same on an infinite surface. The energetics of the actual dissociation process has been studied later explicitly [38] with the semiempirical MO method SINDO1 [39–41]. In this work the reaction pathway from adsorption of the water molecule via the oxygen atom to the four-fold coordinated Ti atom to the subsequent abstraction of an H atom and its bonding to an adjacent O atom of the surface was studied and the activation barrier explicitly determined.

A reactivity index study to choose the best template for a particular zeolite synthesis was presented by Chatterjee and Iwasaki [42]. The authors modeled the zeolite frame by chains (SiO_4H_4, AlO_4H_5, $Si_2O_7H_6$, $AlSiO_7H_7$, $Si_3O_{10}H_8$, $Si_2AlO_{10}H_9$) and rings ($Si_4O_{12}H_8$, $Si_3AlO_{12}H_9$, $Si_5O_{15}H_{10}$, $Si_4AlO_{15}H_{11}$) of Si and Al containing compounds and the templates by small neutral and cationic organic molecules (formaldehyde, methylamine, methanol, tetramethylammonium cation, tetraethylammonium cation, tetrapropylammonium cation, tetrabutylammonium cation). The goal was to search for an active site in the zeolite frame in order to find the best template. DFT calculations with the BLYP [43,44] exchange-correlation functional were done and the local softness and the Fukui function f extracted. As a guideline they proposed the concept that the interaction of clusters and templates is favorable, if atoms with the largest s^+ or f^+ and atoms with the largest s^- or f^- values are combined. This means electrophilic sites react with nucleophilic sites. From their results they concluded that rings are better than chains for the clusters and small templates are favored over large templates.

4.1.2. Energetics

In a more sophisticated consideration the reactivity of a surface for deposition or solvation processes is directly probed by the energetics of processes which take place at the surface of a solid. Several situations are conceivable: solid–gas, solid–liquid and solid–liquid–gas processes. We present a few selected examples for these different cases of multicomponent system.

In a solid–gas process the deposition of metal atoms on a substrate is an interesting example. For such a case the nucleation process of copper deposition on a magnesium oxide surface was studied [45]. The underlying method was MSINDO [46–48], an improved version of SINDO1. The MgO substrate was modeled by a $(8 \times 8 \times 3)$ $Mg_{96}O_{96}$ free cluster. The optimal arrangements of Cu atoms were determined for one to six Cu atoms (Fig. 7). The first Cu binds to an O atom of the surface. The second atoms binds to an adjacent O atom under formation of Cu–Cu bond. The third and fourth Cu atoms are bound to the surface in such a way that they are located on top of Mg atoms. This is necessary because the dominating factor is the formation of further Cu-Cu bonds. For five Cu atoms the optimal arrangement (Fig. 7d) is achieved by adding a Cu atom to a Cu–Cu bond of the Cu_4 rhombus located over an O atom. Alternatively, a square arrangement (Fig. 7e) is possible with four Cu atoms on top of O atoms and one central Cu atom on top of an Mg atom. The latter arrangement is less stable by only 1 kcal/mol. The Cu atoms are held together via Cu–Cu bonds. A sixth Cu atom is adsorbed on an Mg atom (Fig. 7f) again with a preference for Cu–Cu bonds. Another structure (Fig. 7g) was found at almost the same energy with a difference of 0.1 kcal/mol. Similar structures were found, if one Cu atom was replaced by a Ga atom [49]. The Cu atoms dominate the structure of these mixed clusters and consequentially the nucleation process of the intermetallic CuGa phase.

An example for a solid–liquid reaction is the acidic dissolution at the MgO (100) surface. The mechanism of this process has been studied [50] also with the MSINDO method. The MgO solid was simulated by a $(8 \times 8 \times 4)$ $Mg_{128}O_{128}$ cluster surrounded by two layers of pseudoatoms sideways and at the bottom, resulting in a $(12 \times 12 \times 6)$ array. The embedding procedure [21] was discussed in the previous section. In the course of the dissolution reaction, vacancies and protrusions are formed. They are the result of migrations of atoms at the surface. Various mechanism for migration were considered. All consider the protonation of O atoms at the surface as the first step. It was found that the migration of a protonated O atom and an adjacent Mg atom to

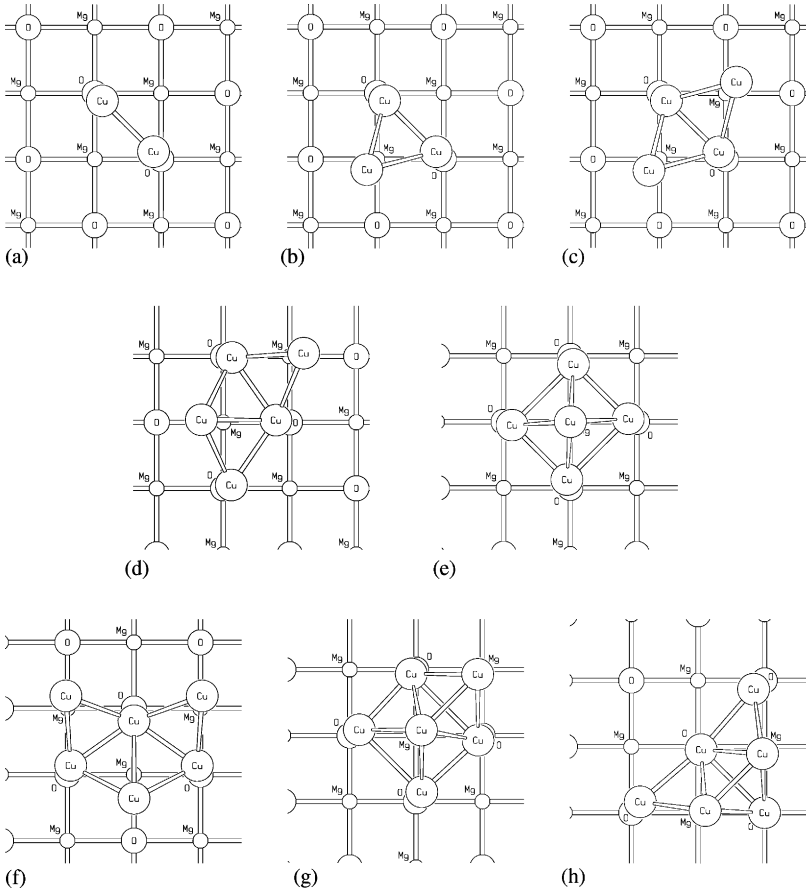

Fig. 7. Structure of adsorbed copper clusters on an MgO (100) surface: Cu_2 (a), Cu_3 (b), Cu_4 (c), Cu_5 (d,e), Cu_6 (f–h).

ex situ positions was a favorable step, i.e., an exothermic process leading to solvated Mg^{2+} and vacancies on the surface.

In a solid–liquid–gas reaction the formation of ZrO_2 on the Si (100) surface from $ZrCl_4$ and H_2O was investigated [51]. The authors modeled this reaction by defining the reaction steps and by optimizing the necessary structures in cluster and periodic calculations. Cluster calculations were carried out with the B3LYP functionals [52,44]. Periodic calculations were carried out in the generalized gradient approximation with the Perdew–Wang PW91 [53] non-local functional. The reaction steps are (i) wet oxidation of the silicon (100) surface, (ii) reaction of gas phase $ZrCl_4$ with the hydroxylated silicon surface, (iii) hydrolysis of the chemisorbed $ZrCl_2$ groups. From the calculations the following conclusions were drawn: The wet oxidation of silicon occurs via migration of H of OH groups and H_2 desorption. Because of the high activation energy there are non-oxidated regions on the surface, which can serve as nucleation centers for the attack of $ZrCl_4$. The gas phase reaction with $ZrCl_4$ has a low activation energy and is slightly exothermic. Zr–OH....Zr bridges are formed after hydrolysis.

4.2. Interfaces

4.2.1. Modeling

In the previous subsection the nucleation process of Cu_n and $Cu_{n-1}Ga$ cluster formation on an MgO surface was described. A similar approach was taken to describe the energetics and bonding properties of the Ni/β-SiC (001) interface [54], a system of interest because of its technological importance. The authors emphasized that the knowledge of the reactivity and of the electronic structure of the metal-semiconductor interface is the first step towards device design. As the epitaxial growth of ultrathin metal films on a substrate is hampered by the mismatch between the lattice constants of the film and the substrate, it is important to search for the stabilization of metastable phases with strong adhesion energy and close matching conditions. The Ni/SiC system was considered as a suitable system. A full-potential linearized augmented plane wave (FLAPW) method in the local density approximation of DFT was used. The Ni/SiC (001) interface was modeled by an Ni monolayer on a SiC substrate slab that consists of seven (six) layers of Si and six (seven) layers of C for the Si (C) terminated surface. There are four possible adsorption sites for Ni

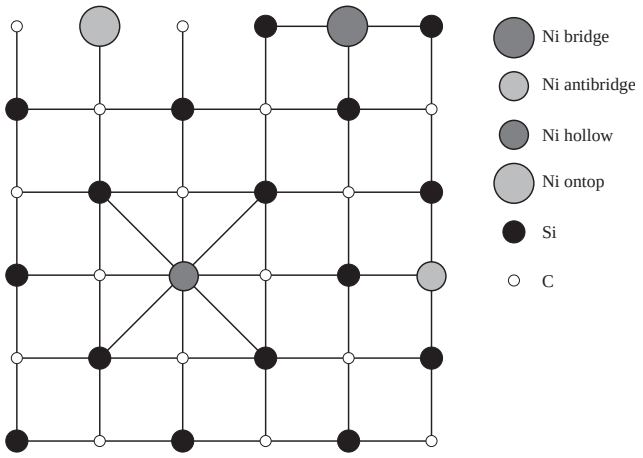

Fig. 8. Adsorption sites of Ni atoms on the SiC (001) surface.

atoms: bridge, anti-bridge, four-fold (hollow) and on-top sites (Fig. 8). A high adsorption energy of 6.6–7.4 eV for adsorption of Ni was found at all adsorption sites except the on-top sites, both for adsorption at the Si terminated and the C terminated surface. It was concluded that the SiC (001) surface is highly reactive for Ni and therefore suitable for the growth of metallic Ni and the formation of Ni silicides.

A closer inspection of intrinsic interfaces was given in a study of the electronic structure of twist grain-boundaries in ZnO and the effect of Sb doping [55]. The computational method was plane wave pseudopotential DFT. The generalized gradient approximation (GGA) level with the exchange-correlation functional by Perdew et al. [53] was employed. Grain boundaries were generated by twisting of a (0001) plane. Two different twist grain boundaries were investigated. One grain boundary was generated by a rotation where the grain boundary plain cut across the polar Zn–O bonds and the other grain boundary resulted from a rotation through the non-polar Zn–O bonds. A grain boundary energy was defined and the second grain boundary was identified as the more stable one. It was also found that the density-of-states (DOS) curves for the boundary system and the bulk are very similar. Doping of the bulk with Sb did not lead to major distortions of the structure. However, in the grain boundary the impurity caused displacements of 0.13 Å for both of the nearest neighbor Zn and O atoms. The grain boundary fostered electron localization between Sb and the neighboring Zn, which led to the formation of a weak bond between these atoms. The localization of charge suggested an increase in cohesion at the interface.

4.2.2. Energetics

If one wants to follow a reaction process more closely, one must apply a molecular dynamics method. Such a study was presented for binary (hydr)oxide systems under mechanical stress [56]. The goal was the elucidation of the reaction mechanism which leads to the formation of a heterometalloxane bonds. The considered reacting systems were SiO_2 and $Ca(OH)_2$ under the assumption of OH groups at the surface of SiO_2. If mechanical stress was applied on the combined system, reactive dehydration and amorphization was observed. The authors presented a mechanism where an H atom from an OH group of the acidic solid (SiO_2) and OH group of the basic solid ($Ca(OH)_2$) are eliminated as H_2O and the remaining O of the acidic solid forms a bond to the basic solid. They introduced two models for the simulation. The first model consisted of two small clusters $(SiO_4H_2)^{2-}$ and $Ca(OH)_6^{4-}$ and they calculated the overlap between H_{Si} and O_{Ca} with the DFT Xα method. They found that the overlap charge increased with decreasing distance between these atoms. In the second model much larger clusters were employed, but the subsequent molecular dynamics was carried out with an analytical potential of Born–Mayer–Huggins type to describe the surface relaxation. A more advanced quantum chemical treatment was beyond reach. The calculations supported the following mechanism. The first step is the proton transfer of OH of SiO_2 to the OH of $Ca(OH)_2$. This results in water cleavage and dehydration. Finally the Ca atom moves to form a Ca–O–Si bridge bond.

4.3. Bulk

4.3.1. Indices and modeling

It was up to Dronskowski [57] to extend the Parr–Pearson concept of reactivity [12] to solid-state materials and to implement it in the Extended Hückel approximation [58]. The total electronic energy, which is equivalent to the total energy on the Extended Hückel level, is given up to the Fermi energy ε_F as

$$E = \int \mathrm{d}\mathbf{k} \int^{\varepsilon_F} \mathrm{d}\varepsilon (E_{\mathrm{diag}}(\varepsilon, \mathbf{k}) + E_{\mathrm{ndiag}}(\varepsilon, \mathbf{k})), \tag{13}$$

where E_{diag} and E_{ndiag} are diagonal and non-diagonal contributions, respectively. The hardness η is approximated as

$$\eta \approx \frac{1}{2}(E^+ + E^-) - E^0. \tag{14}$$

A suitable arrangement of the terms resulting from a combination of (13) and (14) leads to a partioning of η as a sum of atomic reactivity increments ζ_R:

$$\eta = \sum_R \zeta_R = \sum_R (\zeta_{R,\mathrm{net}} + \zeta_{RR'\mathrm{bond}}). \tag{15}$$

The ζ_R consist of net atomic reactivity increments $\zeta_{R,\mathrm{net}}$ and bond reactivity increments $\zeta_{RR'\mathrm{bond}}$. From these electrophilic (acidic) and nucleophilic (basic) reactivity

indices can be defined. The scheme was applied to the acid–base solid-state reaction from $K_2Ti_4O_9$ to $K_2Ti_8O_{17}$. The goal was to analyze all atoms with respect to their electronic reactivity, acidity and basicity and to identify the most basic oxygen atom. It was found that the changing connectivity of this atom governs the structural changes from $K_2Ti_4O_9$ to $K_2Ti_8O_{17}$.

In another study Dronskowski and Hoffmann [59] investigated the chemical character of Mo–Mo, Mo–X and A–X bonds in AMo_3X_3 phases ($A = \mathrm{Li, Na, K, In}$; $X = \mathrm{Se, Te}$). For this purpose Extended Hückel calculations were performed for the systems and bond reactivity, electrophilicity and nucleophilicity determined. These predict that the Mo–Mo bond is chemically inert, the A–X bond has a high acidity and is easily attacked by Lewis bases and that the Mo–X bonds show high basicity and are suitable targets for strong Lewis acids.

Another indirect approach to reactivity is offered by a mechanistic study of the ternary systems consisting of titanium, silicon and nitrogen [60]. The goal is the preparation and characterization of Ti–Si–N ternary powders and thin films. Starting materials are $Ti(NMe_2)_4$ and SiH_4 which react and eventually yield TiN and Si_3N_4 mixtures. The various steps of their model involve intermediates $HTi(NMe_2)_3$ on one hand and $H_3Si(NMe_2)_3$, $H_2Si(NMe_2)_2$ and $HSi(NMe_2)_3$ on the other hand. In a phase diagram (Fig. 9) the upper part shows the composition portion of the model approach. The calculations were on the ab initio level. Geometries were optimized on the Hartree–Fock level with the 3–21G basis set. Energies were evaluated on the MP2 level. To save computer time the NH_2 group was replaced by H in some model compounds. The transition states between the aforementioned intermediates were calculated. The activation energies were taken as a measure of the chemical reactivity. Since the barriers for the reagent SiH_4 was larger than for H_3SiNH_2, which in turn was larger than for $H_2Si(NH_2)_2$, the reactivity was said to increase in this sequence. This means, if the reaction has been successfully started, it will proceed more easily through the following steps.

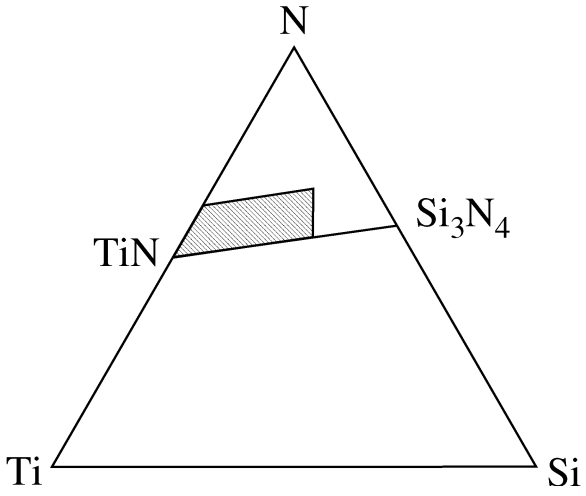

Fig. 9. Schematic representation of the relevant portion of the phase diagram of the Ti–Si–N system.

4.3.2. Energetics

Direct approaches to the reactivity of solids have to consider the actual situation in the bulk. Here diffusion plays the decisive role. A diffusion mechanism can take place via vacancies or interstitials, but less likely via direct exchange (Fig. 10).

We start with the consideration of self-diffusion in the bulk. A suitable case is the diffusion in β-LiAl via vacancies [61]. The bulk was modeled by a series of free clusters with up to 212 atoms. They were arranged in a shell-like structure around an Li or Al vacancy, respectively. Three different processes were considered: the migration of an Al atom to an adjacent Al vacancy, the migration of an Li atom to an adjacent Li vacancy and the migration of Li to an Al vacancy. Structure and energy of equilibrium and transition state were calculated with SINDO1 [39,40]. The results on the unrelaxed bulk excluded the Al to Al vacancy migration as a possibility because of a very high activation energy of about 80 kcal/mol. The Li to Li vacancy migration showed a small barrier of 10 kcal/mol. But the Li to Al vacancy migration proceeded without a barrier. The last two processes were then investigated under relaxation of the innermost shell of 20 atoms. The qualitative result did not change, i.e., a small barrier for Li to Li vacancy

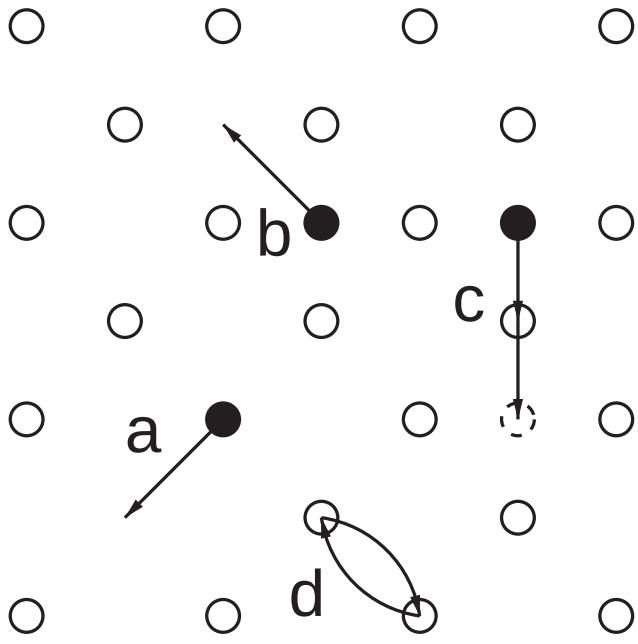

Fig. 10. Diffusion mechanisms: (a) vacancy, (b,c) interstitial, (d) direct exchange.

migration and no barrier for the Li to Al vacancy migration was found. The explanation was that the Li atom has a sterically more favorable pathway in the second case through a six-membered ring of three Li and three Al atoms than in the first case through a six-membered ring of six Al atoms. After the migrating Li has reached an Al vacancy, it leaves an Li vacancy for further Li migration. The calculated net charges on the atoms were in the order of 0.1 so that an explanation via a charge driven migration would not be appropriate.

If one wants to know more about the details of the diffusion process, a molecular dynamics (MD) approach like the Car–Parrinello method [62] can be quite useful. Such a study was undertaken on Li_3N by Sarntheim et al. [63]. The MD method was implemented in the periodic projector-augmented-wave (PAW) method [64]. As a model a hexagonal supercell of 32 atoms was chosen. The goal was the determination of the barriers for lithium jumps to adjacent vacancies. The diffusion in the Li_2N plane had an extremely low barrier of 0.004 eV, whereas it was two orders of magnitude larger perpendicular to the Li_2N plane. In contrast to the previous case the lattice was much more ionic, so that the mechanism is driven by Li ions. The in-plane motion creates the suitable vacancies, but the rate-limiting step is the jump between planes. Typical trajectories for the in-plane motion were presented and mean-square displacement of a vacancy in-plane and between planes was shown in dependence of time.

A more complicated system, the ternary $Li_{2-2x}Mg_{1+x}Si$ crystal ($x \sim 0.06$) was studied by Wengert et al. [65]. Here the ionic diffusion in a novel superionic conductor was the goal of the investigation. The model was a $(2 \times 2 \times 2)$ supercell with periodic boundary conditions. The local density approximation (LDA) in DFT was used and a Car–Parrinello MD simulation performed. Various defective structures were chosen as starting configurations for MD calculations at 600, 900 and 1400 K. The mean-square displacement for the three species Li, Mg and Si were determined as a function of time. It was found that the migration of Li is favored, but Mg migration is also possible, whereas Si is not involved in this process. The diffusion mechanism is characterized as defect mechanism which involves migration of vacancies.

Whereas the diffusion of Li was no surprise in the discussed cases, it is more difficult to predict the migrating species in other systems. The self-diffusion of Si in $TiSi_2$ was studied by tight-binding MD [66]. The formation of $TiSi_2$ is obtained by solid-state reaction. In experiments a Ti layer is deposited on top of the silicon substrate and the silicide formation is then activated by a thermal treatment. To understand the growth of the silicide at the Ti/Si interface, the mobile species for diffusion must be determined. The crystalline structure was modeled by orthorhombic cells and treated with a tight-binding potential incorporated in a periodic program. The MD simulation was done with the Parrinello–Rahman algorithm [67] and the Nose algorithm [68]. The MD calculations at 2500 and 2900 K showed that the Si is the moving species, whereas the Ti sublattice remained initially fixed. After the Si atom remained at an interstitial position for a longer time, the Ti atoms began to move to enable the Si migration through the Ti sublattice.

Another DFT study on the GGA level with plane waves describes the diffusion of oxygen in SiO_2 [69]. The background is a model which postulates that gas-phase oxygen diffuses through the growing SiO_2 layer and reacts at the Si/SiO_2 interface. A supercell based on the α-quartz structure was chosen to study the "impurity" O in SiO_2. The Car–Parrinello method was again chosen for MD simulation. However, an extremely large number of plane waves were required to accurately describe the O valence wave functions which are highly localized. The additional O atom was initially located at an interstitial position. It was found that it migrates to form a peroxy linkage configuration. Parallel calculations were carried out for O_2. Here O_2 remained close to the initial interstitial site while adjacent O atoms in the bonded net work relaxed outward. The energies of the O_2 and the O in peroxy linkage were almost equal. The author speculated that a migration of the peroxy linkage is possible.

Doping of materials by other atoms can change the properties of materials and the understanding of the accompanying process is important. In this way a study of boron diffusion in silicon was motivated [70]. A boron atom was placed into two Si cells of different size with 64 and 216 atoms, respectively, in the diamond lattice. Again a DFT tight-binding method was invoked and an MD study performed. The minimum structure was obtained as a configuration, where the B atom and an Si atom share a lattice site, both sitting at interstitial positions. Trajectories for the MD simulation were calculated. From the results it was predicted that the B atom catches an Si atom at an interstitial site. An oscillation starts, until the B atom evades to an interstitial site. From there it can reach another lattice site and receive another Si atom. In this way the B atom can migrate through the lattice. Diffusion coefficients and energies for migration were determined.

Another paper on the same problem considers not only a single B atom, but also clusters of B_2Si up to $B_{12}Si_7$ [71]. Again a density functional tight-binding method [72] was used. But LDA and GGA calculations were performed with VASP [73], a DFT program based on plane waves. The bond energy of interstitial B–Si pairs were calculated. Different diffusion pathways of B atoms were compared by migration barriers. It was found that the migration occurs via neutral pairs. The clusters B_2Si up to $B_{12}Si_7$ were studied with atoms at

interstitial positions. Again it was found that the diffusion of a B atom is mediated by interstitials. This process can occur in one or two steps. The importance of larger clusters at higher temperatures was considered.

An even more sophisticated problem is the investigation of phase transition. Such a study was presented on the pressure-induced frustration and disorder in $Mg(OH)_2$ and $Ca(OH)_2$ by Raugei et al. [74]. Starting point for the study was the reversible disorder of the H sublattice in $Mg(OH)_2$ under pressure, which was observed by an IR line broadening. Periodic DFT calculations with plane waves were performed. A molecular dynamics simulation and a pressure simulation were included. The pressure-induced transition from the crystalline to the amorphous state under pressure was simulated by decrease of the interlayer distance. During this process, the arrangement of the OH groups changed in such a way that the initial symmetry was lost. The amorphization was explained by a combination of electrostatic effects and short-range repulsion.

5. Final remarks

We have presented a review on the present day possibilities of quantum chemistry to deal with the reactivity of solids. No attempt for completeness has been made, rather the various approaches have been explained by the discussion of special, but typical examples. No weighting of the importance of the discussed cases or of the used method is implied. The indirect approach by reactivity indices is followed by an indirect approach of modeling solid-state reactions by molecular reactions. A direct approach offers an energetic study of a reaction pathway in the solid. Here diffusion processes are most important and were studied without and with molecular dynamics simulation. Phase transitions are a challenge for the future.

Acknowledgments

This research was partially supported by Deutsche Forschungsgemeinschaft.

References

[1] J. Falbe, M. Regitz, Römpp Chemie Lexikon, 9. Aufl., Georg Thieme, Stuttgart, New York, 1995.
[2] N. Svartholm, Ark. Kemi Mineral. Geol. A 15 (13) (1941) 1.
[3] R. Daudel, A. Pullman, C. R. Acad. Sci. 220 (1945) 888.
[4] R. Daudel, C. Sandorfy, C. Vroelant, P. Yven, O. Chalvet, Bull. Soc. Chim. Fr. 17 (1950) 66.
[5] C.A. Coulson, Proc. R. Soc. London Ser. A 169 (1939) 413.
[6] C.A. Coulson, Faraday Soc. Disc. 2 (1947) 9.
[7] F.H. Burkitt, C.A. Coulson, H.C. Longuet-Higgins, Trans. Faraday. Soc. 45 (1951) 373.
[8] K. Fukui, T. Yonezava, H. Shingu, J. Chem. Phys. 20 (1952) 722.
[9] K. Fukui, Theory of Orientation and Stereoselection, Springer, Berlin, Heidelberg, New York, 1975, p. 34ff.
[10] K. Jug, A.M. Köster, J. Phys. Org. Chem. 3 (1990) 599.
[11] M.S. Gopinathan, K. Jug, Theor. Chim. Acta 63 (1983) 497, 511.
[12] R.G. Parr, R.G. Pearson, J. Am. Chem. Soc. 105 (1983) 7512.
[13] W. Yang, R.G. Parr, Proc. Natl Acad. Sci. USA 82 (1985) 6723.
[14] R.G. Pearson, J. Am. Chem. Soc. 85 (1963) 3533.
[15] R.G. Parr, W. Yang, J. Am. Chem. Soc. 106 (1984) 4049.
[16] R.G. Parr, W. Yang, Density-Functional Theory of Atoms and Molecules, Oxford University Press, New York, 1989, p. 10ff.
[17] P. Politzer, D.G. Truhlar, Chemical Application of Atomic and Molecular Electrostatic Potentials, Plenum, New York, London, 1980.
[18] J.S. Murray, K. Sen, Molecular Electrostatic Potentials, Elsevier, Amsterdam, 1996.
[19] K. Jug, G. Geudtner, Chem. Phys. Lett. 208 (1993) 537.
[20] M. Krack, T. Bredow, K. Jug, Chem. Phys. Lett. 237 (1995) 250.
[21] T. Bredow, G. Geudtner, K. Jug, J. Chem. Phys. 105 (1996) 6395.
[22] J. Noga, P. Banacký, S. Biskupic, R. Boca, P. Pelikan, M. Svrcek, A. Zajac, J. Comput. Chem. 20 (1999) 253.
[23] T. Bredow, G. Geudtner, K. Jug, J. Comput. Chem. 22 (2001) 89.
[24] F. Janetzko, T. Bredow, K. Jug, J. Chem. Phys. 116 (2002) 8994.
[25] A.M. Dobrotvorskii, R.A. Evarestov, Phys. Stat. Sol. (B) 66 (1974) 83.
[26] R.A. Evarestov, Phys. Stat. Sol. (B) 72 (1975) 569.
[27] C. Pisani, R. Dovesi, C. Roetti, Hartree-Fock Ab Initio Treatment of Crystalline Systems, in: Lecture Notes in Chemistry, Vol. 48, Springer, Berlin, Heidelberg, New York, 1988.
[28] B.G. Köhler, P.A. Coon, S.M. George, J. Vacuum Sci. Technol. B 7 (1989) 1303.
[29] F. Bozso, A. Avouris, Phys. Rev. B 38 (1988) 3937.
[30] F. Bozso, A. Avouris, Phys. Rev. Lett. 57 (1986) 1185.
[31] M.F. Jarrold, Y. Ijiri, U. Ray, J. Chem. Phys. 94 (1991) 2618.
[32] J.M. Alford, R.T. Laaksonen, R.E. Smalley, J. Chem. Phys. 94 (1991) 2618.
[33] M. Krack, K. Jug, Chem. Phys. 192 (1995) 127.
[34] M. Krack, K. Jug, in: J.S. Murray, K. Sen (Eds.), Molecular Electrostatic Potentials: Concepts and Applications, Elsevier, Amsterdam, 1996, p. 197.
[35] R.F. Nalewajski, in: K. Sen (Ed.), Structure and Bonding: The Chemical Hardness, Vol. 80, Springer, Heidelberg, 1993, p. 115.
[36] R.F. Nalewajski, J. Korchowiec, Z. Zhou, Int. J. Quantum Chem. Quant. Chem. Symp. 22 (1988) 349.
[37] R.F. Nalewajski, A.M. Köster, T. Bredow, K. Jug, Mol. Catal. 82 (1993) 407.
[38] T. Bredow, K. Jug, Surf. Sci. 327 (1995) 398.
[39] D.N. Nanda, K. Jug, Theor. Chim. Acta 57 (1980) 95.
[40] K. Jug, R. Iffert, J. Schulz, Int. J. Quantum Chem. 32 (1987) 265.
[41] J. Li, P. Correa de Mello, K. Jug, J. Comput. Chem. 13 (1992) 85.
[42] A. Chatterjee, T. Iwasaki, J. Phys. Chem. A 105 (2001) 6187.
[43] A. Becke, J. Chem. Phys. 88 (1988) 2547.
[44] C. Lee, W. Yang, R.G. Parr, Phys. Rev. B 37 (1988) 785.
[45] G. Geudtner, K. Jug, A.M. Köster, Surf. Sci. 467 (2000) 98.
[46] B. Ahlswede, K. Jug, J. Comput. Chem. 20 (1999) 563.
[47] B. Ahlswede, K. Jug, J. Comput. Chem. 20 (1999) 572.
[48] T. Bredow, G. Geudtner, K. Jug, J. Comput. Chem. 22 (2001) 861.
[49] G. Geudtner, K. Jug, Z. Anorg. Allg. Chem. 629 (2003), in press.
[50] D.J. Simpson, T. Bredow, R.St.C. Smart, A.R. Gerson, Surf. Sci. 516 (2002) 134.
[51] V.V. Brodskii, E.A. Rykova, A.A. Bagatur'yants, A.A. Korkin, Comput. Mater. Sci. 24 (2002) 278.
[52] A.D. Becke, J. Chem. Phys. 98 (1993) 5648.

[53] J.P. Perdew, S. Chevary, S. Vosko, K. Jackson, M. Pederson, D. Singh, C. Fiolhais, Phys. Rev. B 46 (1992) 6671.
[54] G. Profeta, A. Continenza, A.J. Freeman, Phys. Rev. B 64 (2001) 045303.
[55] H.S. Domingos, P.D. Dristowe, Comput. Mater. Sci. 22 (2001) 38.
[56] M. Senna, Y. Fujiwara, T. Isobe, J. Tanaka, Solid State Ion. 141–142 (2001) 31.
[57] R. Dronskowski, J. Am. Chem. Soc. 114 (1992) 7236.
[58] R. Hoffmann, J. Chem. Phys. 39 (1963) 1397.
[59] R. Dronskowski, R. Hoffmann, Inorg. Chem. 31 (1992) 3107.
[60] X. Liu, Z. Wu, H. Cai, Y. Yang, T. Chen, C.E. Vallet, R.A. Zuhr, D.B. Beach, Z.-H. Peng, Y.-D. Wu, T.E. Concolino, A.L. Rheingold, Z. Xne, J. Am. Chem. Soc. 123 (2001) 8011.
[61] G. Geudtner, A.M. Köster, K. Jug, Ber. Bunsenges. Phys. Chem. 102 (1998) 833.
[62] R. Car, M. Parrinello, Phys. Rev. Lett. 55 (1985) 2471.
[63] J. Sarntheim, K. Schwarz, P.E. Blöchl, Phys. Rev. B 53 (1996) 9084.
[64] P.E. Blöchl, Phys. Rev. B 50 (1994) 1753.
[65] S. Wengert, R. Nesper, W. Andreoni, M. Parrinello, Phys. Rev. Lett. 77 (1996) 5083.
[66] M. Ianuzzi, P. Raiteri, L. Migho, Comput. Mater. Sci. 20 (2001) 394.
[67] M. Parrinello, A. Rahman, J. Chem. Phys. 76 (1982) 2662.
[68] S. Nose, L. Klein, Mol. Phys. 50 (1983) 1055.
[69] D.R. Hamann, Phys. Rev. Lett. 81 (1998) 3447.
[70] W. Windl, R. Stumpf, X.-Y. Liu, M.P. Masquelier, Comput. Mater. Sci. 21 (2001) 496.
[71] P. Alippi, L. Colombo, P. Ruggerone, Comput. Mater. Sci. 22 (2001) 44.
[72] D. Porezag, T. Frauenheim, T. Koehler, G. Seifert, R. Kaschner, Phys. Rev. B 51 (1995) 12947.
[73] G. Kresse, J. Hafner, Phys. Rev. B 47 (1993) 558.
[74] S. Raugei, P.L. Silvestrelli, M. Parrinello, Phys. Rev. Lett. 83 (1999) 2222.